

We are IntechOpen, the world's leading publisher of Open Access books Built by scientists, for scientists

6,900

Open access books available

186,000

International authors and editors

200M

Downloads

Our authors are among the

154

Countries delivered to

TOP 1%

most cited scientists

12.2%

Contributors from top 500 universities



WEB OF SCIENCE™

Selection of our books indexed in the Book Citation Index
in Web of Science™ Core Collection (BKCI)

Interested in publishing with us?
Contact book.department@intechopen.com

Numbers displayed above are based on latest data collected.
For more information visit www.intechopen.com



Aluminium 7020 Alloy and Its Welding Fatigue Behaviour

Carlos Bloem¹, Maria Salvador², Vicente Amigó² and Mary Vergara¹

¹Universidad de Los Andes

²Universidad Politécnica de Valencia

¹Venezuela

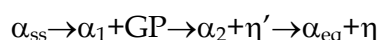
²España

1. Introduction

Since Alfred Wilm discovered the aluminium alloys hardening precipitation phenomena at the beginning of the last century (Polmear 1996), the use of aluminium alloys has increased, owing their advantages against corrosion and good strength weight ratio.

The Aluminium Zinc Magnesium ternary alloys are getting more relevance every day. These alloys are commonly called Al-Zn-Mg. In this family the most used are the AA7005 and AA 7020, which are nearly the same alloys. Although the most remarkable difference between them is the slightly better mechanical behaviour of the 7020 one after welding.

The ageing development of these alloys follows a simple precipitation phenomena summarized as:



Some investigators propose a transitional step on the Guinier Preston (GPs) evolution that gives the response to the natural ageing as:



The calorimetric study of the natural ageing evolution shows that there is no difference on the heat exchange of η' and η . So, the GPs evolution is the responsible of strengthening of the alloy.

The mechanical properties of AA7020 are evaluated and the exponential evolution is advisable, due to natural ageing.

The fatigue behaviour of AA7020 natural aged shows a typical Aluminium Wohler pattern. From this curve a mathematical model is proposed.

Welded aluminium:

Riveted and welded aluminium structures are getting more relevance every day.

Heat treatable alloys as the 7XXX, 2XXX, and 6XXX are vulnerable to critical changes in the Heat Affected Zone (HAZ) due to the heat input during welding. For this reason an extensive study of the HAZ is done.

This chapter attempts to describe the changes happening during the welding process of AA7020.

A concise study of the HAZ by Differential Scanning Calorimetry (DSC) and Transmission Electron Microscopy (TEM) is presented. Likewise a fatigue study is done.

The fatigue pattern of the welded joints looks like parent metal with a significant decrease of its strength. From this data, a mathematical model for the fatigue behaviour of the welded joint is developed.

2. Ageing (Heat treatment)

Aluminium Zinc Magnesium ternary alloys are widely used in medium and large structures. Some of these structures are assembled as factory received with no importance on the alloy heat treatment condition.

The thermal state of the heat treatable aluminium alloys confers important changes to their performance so it is real of importance to take care of it.

Thermal state means how the second phases are precipitated into the aluminium matrix.

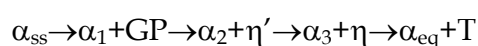
The elementary thermal states are usually designated by the letter T followed by a number as described below: (alubook, 2010)

- T1: Cooled from an elevated temperature shaping process and naturally aged to a substantially stable condition.
- T2: Cooled from an elevated temperature shaping process, cold worked and naturally aged to a substantially stable condition.
- T3: Solution heat-treated, cold worked and then naturally aged to a substantially stable condition.
- T4: Solution heat-treated and naturally aged to a substantially stable condition.
- T5: Cooled from an elevated temperature shaping process and then artificially aged.
- T6: Solution heat-treated and then artificially aged.
- T7: Solution heat-treated and over aged stabilised.
- T8: Solution heat-treated, cold worked and then artificially aged.
- T9: Solution heat-treated, artificially aged and then cold worked.

Commercial plates come normally on the T5 or T6 state, but when it is necessary a solution treatment is done. Then, within a few days plates become as stronger as T6. This process is discussed in the next chapter. The microstructural evolution of the alloy is of course the main factor of the mechanical properties enhancement. Such aspect is one of the principal goals of this chapter.

Natural ageing, as artificial ageing is the precipitation of the second metastable phases. Certainly, natural ageing requires more time to evolve the precipitation phenomena. This delay is the response to the slower diffusion process due to the lower temperature.

The basic precipitation process is proposed by many authors as:



However, as discussed onwards, there is a transitional step on GP evolution as follows:



The importance of precipitates evolution is due they are the responsible of strength increase, but only the precipitates that are coherent with aluminium matrix, as seen on figure 1 b) because they block the dislocation movement. On the other hand the precipitates that are not coherent with the matrix are nearly like a void in the dislocation passage.

Figure 1 shows schematically how a solute stays a) dissolved in a solid solution, b) forming a second phase that is coherent with the matrix crystalline structure or c) a precipitate that is not coherent with the structure.

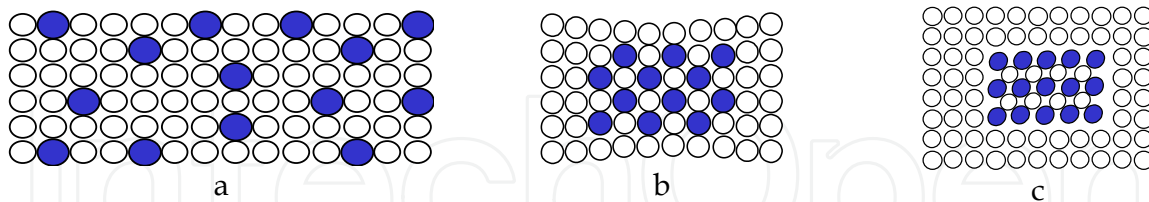


Fig. 1. Diagram of the different states of the solute into the matrix a) supersaturated solution b) precipitate coherent with the matrix c) precipitate incoherent.

It is essential to mention that a precipitate that is not coherent with the aluminium matrix is nearly the same as a filled void, likely as a hole. So the dislocations pass easily through the cavity.

Some second phases are semi-coherent meaning that is coherent in some lattices and incoherent in others.

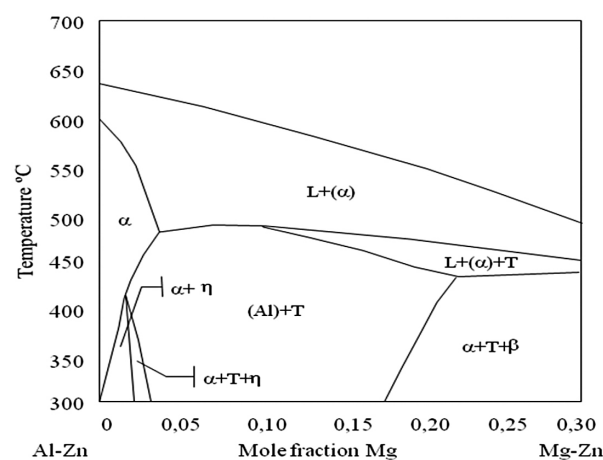


Fig. 2. Isoleth of the Al-5%Zn-Mg alloy

The ternary equilibrium diagram of an Al-Zn-Mg alloy was determined initially by Körser and improved by Mondolfo (Polmear 1996). Nowadays, articles about this diagram still continue explaining, the behaviours, precipitation sequences, temperatures and energies of formation and dissolution of second metastable phases and new heat treatments (Polmear 1996, Schiller et al., 2006, Soto et al., 2007)

Observing the isopleths of the alloy, figure 2 shows that there are two phases; the binary $MgZn_2$ generally called η and the most stable the ternary $Mg_3Zn_3Al_2$ called T. Obviously, there are more intermediate phases between them as mentioned in the precipitation sequence.

The second phases that appear due to its commonly alloying elements in the commercial Al-Zn-Mg alloys are written in table 1.

Because the precipitation process drives the alloy hardening, it is essential to know it. When the solute precipitates in a special manner, the second phases can rise the strength of the alloy more than three times than the quenched condition, the aim of the investigators is to develop heat and or thermo-mechanical treatments that increase the strength.

Element	Designation	Phase
Mg	η, T	$MgZn_2, (AlZn)_{49}Mg_{32},$ $Al_3Mg_2, Al_{12}Mg_{17}$
Si	β	Mg_2Si
Fe		$FeAl_3, (FeCr)_3SiAl_{12}$
Mn		$(FeMn)Al_6$
Cu	α, S	Solid Solution, Al_2CuMg
Cr		$(FeCr)_3SiAl_{12}$
Zr		Solution inside of $(FeMn)Al_6$

Table 1. Commonly second phases found in 7XXX series.

It is necessary start from a supersaturated solid solution to reach a satisfactory hardening after a heat treatment. Heat treatments precipitate the excess of solute in the solid solution as second phases, which generally are metastable. The precipitation goal is that the precipitates must be coherent with the aluminium solid solution.

Precipitation is analogue to solidification. It requires a nucleation and a growth process, on which the alloy goes to a lower thermodynamic state. This equilibrium can be accelerated or damped by mechanical or thermal barriers.

Notwithstanding the ageing treatment, there are many thermo-mechanical treatments, which improve the strengths achieved with only ageing.

3. Natural ageing

3.1 Precipitation evolution

The precipitation evolution of the alloy gives it better mechanical properties. At low temperature (room temperature) 18 ~ 22° C, natural ageing evolves slowly. So, in few weeks natural ageing reaches strength values as its artificial counterpart. This difference in time is due to the lower diffusion rate.

Table 2 shows the evolution in the first stages of the common mechanical properties, where an increase of strength is advisable, while ductility remains nearly the same.

Ageing time (h)	$\sigma_{0,2\%}$ (MPa)	σ_{Max} (MPa)	Elongation (%)
Immediate	141.2	256.3	19.47
1 day	192.5	320.4	18.31
4 days	214.6	349.8	18.99
8 days	224.2	365.8	18.25
11 days	226.8	374.2	18.29
21 days	240.9	386.8	17.84
48 days	241.1	395.9	25.38
90 days	249.8	408.9	18.93
18 months	266.7	421.2	16.94

Table 2. Static mechanical properties evolution of AA7020 due to natural ageing.

As shown on table 2, the mechanical properties evolution is important within the first fifteen days. Then, up to 40 ~ 45 days, the increase in strength is quite significant. After this time,

the ageing process slows down. Nevertheless, the elongation remains nearly the same through the whole ageing time.

To evaluate the ageing evolution, a differential scanning calorimetry test is done. Samples are compared to pure 99,998% aluminium. The heating rate is performed a controlled Ar atmosphere at 20°C per minute. As seen in figure 3, the peaks and valleys represent exothermic and endothermic processes, respectively.

The valleys (endothermic curves) from 60 to 190 ~ 200°C reveal a dissolution of the more immature GPs precipitate. The exothermic peaks between 200 to 300°C are the η' and η precipitations, and the peaks from 300 to 360°C are mixture of sub peaks due to the dissolution of all metastable phases as suggested by (Donoso E. 1985).

To minimize any thermal or inertial distortion on the zone of interest, the thermal analyses are done from -20 to 520°C.

Figure 3 shows the thermal evolution of the second phases between 60° to 410°C.

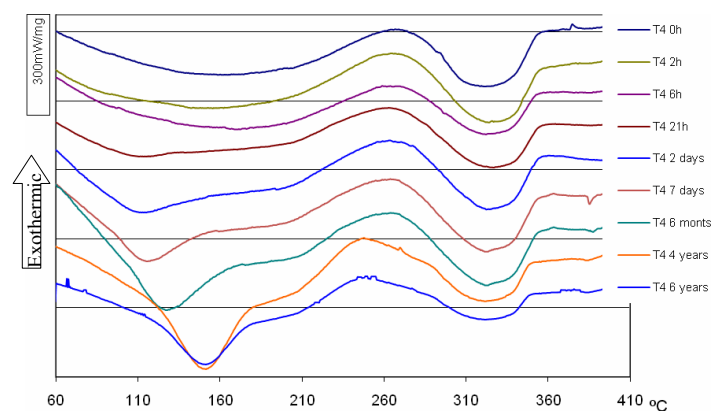


Fig. 3. Thermal evolution of natural ageing precipitation of an AA 7020 alloy.

In the first stages of the precipitation, up to four hours, the precipitate dissolution shows a definitely slow response. In the curve corresponding to 6 hours, there is a slight endothermic peak that can be noticed finishing around 93°C. It is the clear response to small clusters or GP_{Round} dissolutions. On the other hand, observing the 21-hour curve, there are two followed endothermic peaks ending at 90 and 125°C, respectively. Those peaks clearly denote that there are two different dissolution processes and two different precipitates, corroborating the existence of two GPs phases.

From this ageing time and forward, the dissolution peaks show a more stable process due to the increase on the beginning and ending temperatures.

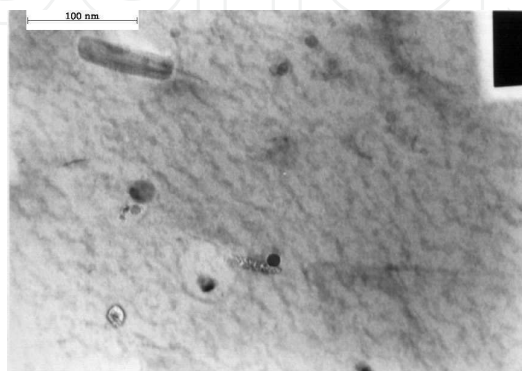


Fig. 4. Rounded GPs on a matrix of aluminium T4 at 25 hours of natural ageing 100,000 X

Figure 4 shows how the GPs evolve after 25 hours of natural ageing. Note the GPs are smaller than 11 nm.

Another point of interest is that through the whole 6 years of ageing process the endothermic and exothermic peaks from 200 to 410°C remain steady. Analyzing the energies in the thermograms, it can be concluded that there are no changes through the ageing process. It obviously construes that in natural ageing the GPs is the only responsible of the alloy hardening increase, because there is no change in the evolution of the zones corresponding to η' and η .

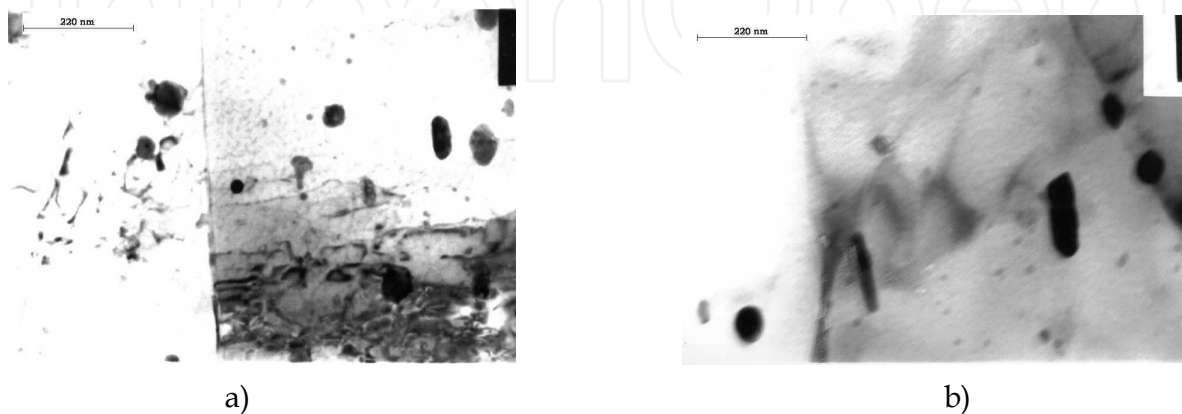


Fig. 5. Precipitation evolution after 90 a) 180 b) days of natural ageing 46,400X

Figure 5 shows how the precipitation evolves. In part *a* of the figure, “coarse” precipitates outshine over the tiny GPs, and in part *b*, Some GPs become bigger than the ones at 90 days. There is relevant to mention that there are no noticeable precipitation free zones (PFZ) surrounding the precipitates in the natural ageing.

3.2 Artificial ageing

Artificial ageing is the most common commercial procedure. The precipitation process is governed by a temperature controlled diffusion process, where the higher the temperature, the faster the atoms move. Special care must be taken on the temperature selection; otherwise, a “burnt” of the alloy can happened.

(Robinson & Tanner et al., 2006, Jiang et al., 2008) and others have found great importance on the quenching rate of Al-Zn-Mg alloys. However, in the case of the AA7020 alloy, the results plotted in figures 6 *a* and *b* show no relevance on the mechanical properties. The largest difference in hardening is less than 2.5%. This can be attributed to the low Cu content of the alloy.

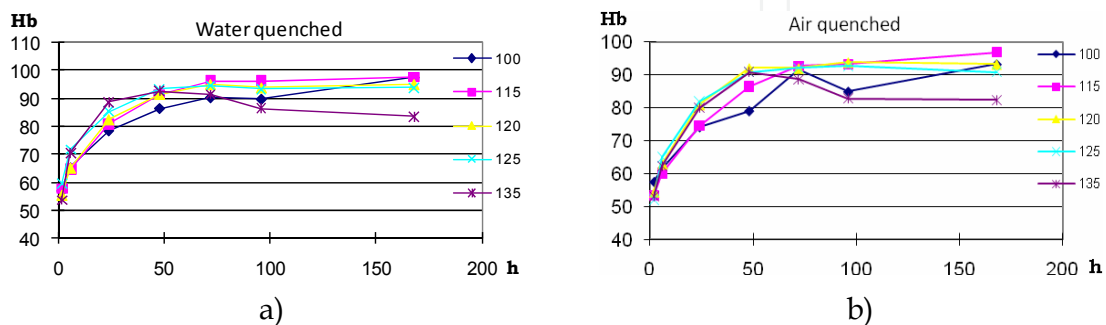


Fig. 6. a, b shows how quenching rate and temperature influences on time and hardness.

Temperature plays an important role on hardening evolution. However, in the first 48 hours (industrial interest) and the range from 120 to 135°C, the highest values of hardening are achieved with both quenching rates. For temperatures above 125°C, the heat treatments cause alloy overageing after 48 hours.

AA 7020 alloys are nearly insensitive to the quenching rate. Nevertheless, it has been found that water quenching make the alloy more unalterable to overageing.

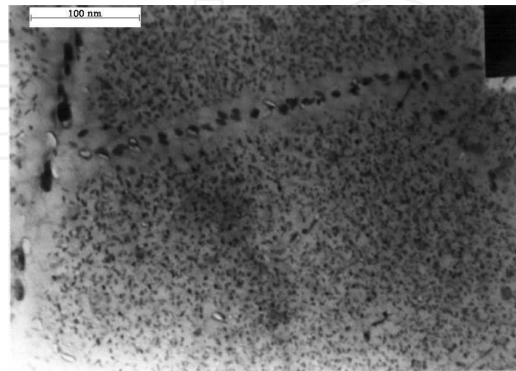


Fig. 7. Aspect of the microstructure after artificial ageing of the AA7020. 100,000X

To ensure no overageing and to reach the more stable thermodynamic condition after the artificial heat treatment, it is required a solubilisation heat treatment, then quench, preferably in water, and finally ageing at 122°C for 48 hours.

The microstructure in the artificial ageing differs of that in the natural ageing. Figure 7 shows a profuse precipitation when the alloy is artificially aged; however, a slightly precipitation free zone also appears in the subgrain boundaries where aligned beads precipitate.

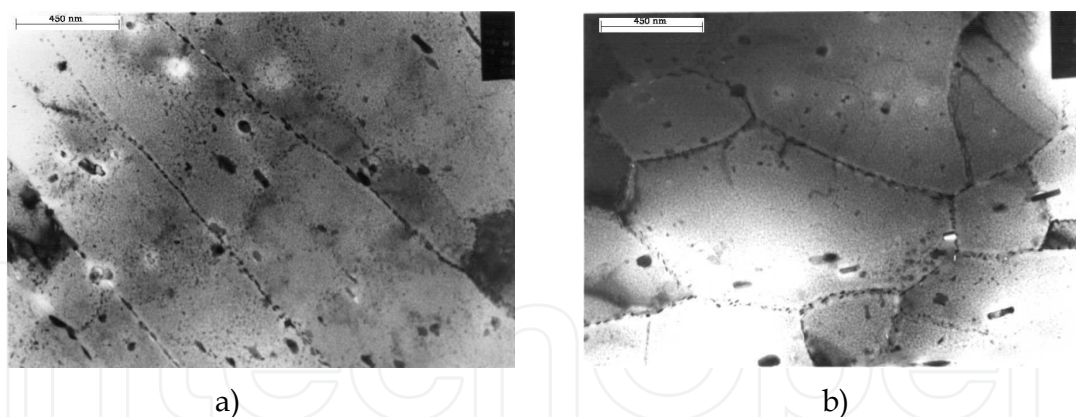


Fig. 8. Differences between the microstructures of AA7020 alloys in T6 a) as delivered and b) after a solution heat treatment TEM 21,500X

In figure 8, a comparison of two micrographs from the alloy in T6; one as-received and the other after a solution heat treatment. Figures 8 a) and b) show the typical texture after lamination, and the equiaxed microstructure after grains recrystallization due to the solution heat treatment, respectively. Certainly, some anisotropy still remains in the as-received material due to the outstretched grains.

Although the precipitation levels for both states are nearly the same, the precipitation of the η' follows the lamination direction in the case of the as-received alloy and a heterogeneous direction in the solubilised one.

4. Fatigue behaviour

Unlike steel, aluminium has no fatigue limit. The fatigue (Wöhler) curve for aluminium follows an exponential pattern, as observed in figure 4.

The fatigue tests are conducted at various stress levels up to fracture in a four-point bending machine. These results are validated with the data obtained from (Gatto F. and Morri E. 1979)

These tests are performed using different plates and time of ageing. The fatigue tests are conducted at room temperature in a not fully reversed loading cycle $R=-0.1$ and frequencies between 3 to 5 Hz.

4.1 Natural ageing fatigue behaviour

Figure 9 shows different fatigue curves for various time of ageing. It is notorious that the ageing time plays an important role in the mechanical properties of the alloy. From the plot, it is advisable that as time of ageing increase, the fatigue resistance decreases considerably at high cycle levels.

The Wöhler curves have a vital importance in mechanical design when fatigue behaviour must be taken into account for engineers.

Curves represented in figure 9 are plotted from the mathematical model discussed in the next paragraph.

The natural ageing evolution of AA7020 shows a contradictory behaviour. The fatigue limit decreases as ageing time evolves, becoming nearly steady after 3 months. This phenomenon is corroborated by the precipitation evolution, as observed in the DSC curves of figure 3. These calorimetric curves show that most of the solute precipitated into GPs; the only difference is the GPs stability reached over time.

The drawback of the fatigue strength decrease is associated to the lower degree of crack propagation resistance caused by the solute distribution and cluster precipitates acting as a brittle phase.

Plasticity is nearly the same in the whole range of ageing time. It is reasonable to suppose that clusters are able to obstruct dislocation movement, but they cannot support high stresses at crack tips. This phenomenon is associated to the residual stresses development when precipitation occurs due to, for example, misalignments, crystalline structure disparity and atomic size differences.

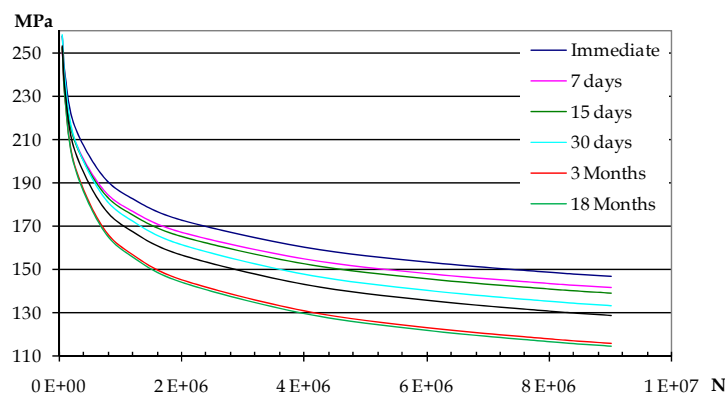


Fig. 9. Fatigue curves of AA7020 at different times of natural ageing.

4.2 Artificial ageing (T6) fatigue behaviour

The fatigue behaviour on high cycles of T6 state shows a slightly better performance than the T4 state with a 30-day or larger natural ageing. It can be attributed to a higher stability and size of the precipitates, which certainly can support better the stresses in front of the crack tip. The T6 fatigue behaviour in high cycles can be up to 10% better than the T4 state. Without any posterior heat input (i.e., welding or grinding), the T6 plates are better than the T4 ones for fatigue loading.

The modelled Wöhler curve and experimental data of the AA7020 T6 is plotted in figure 10.

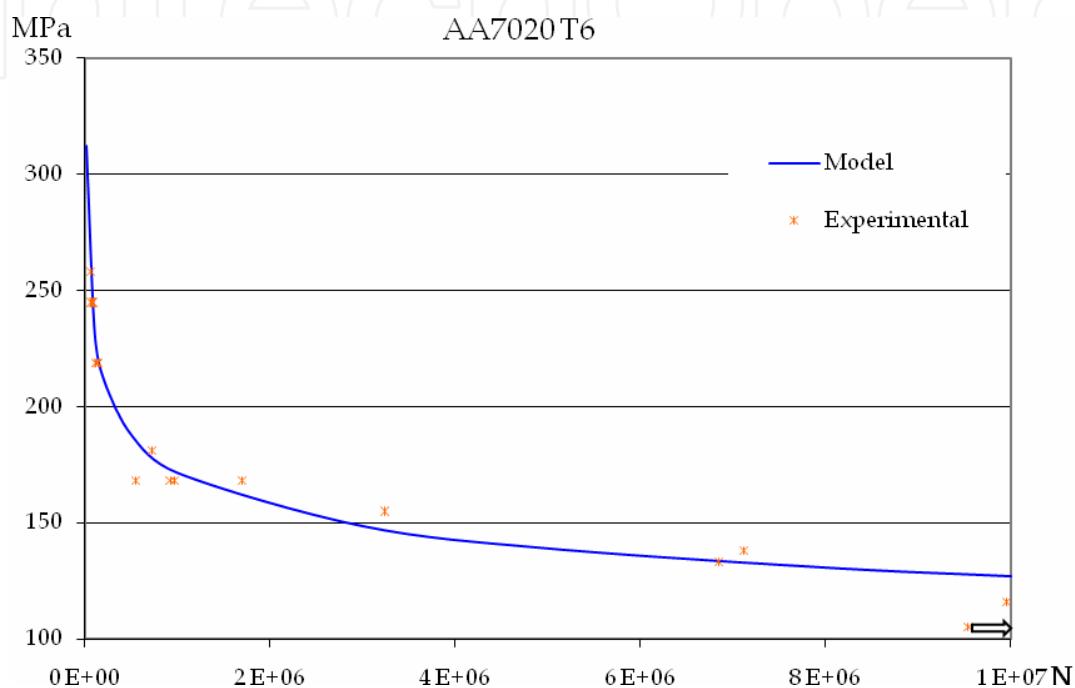


Fig. 10. Fatigue curve of the AA7020 T6

4.3 Mathematical model of fatigue behaviour

The fatigue behaviour of the AA7020 for different thermal states is collected, drawn, and analyzed. Using a least squares approach, a numerical model is found from the experimental data. The best data fit is an exponential equation, written as:

$$\sigma_{(N)} = \sigma_0 * e^{-k * \ln(N)} \quad (1)$$

Where:

$\sigma_{(N)}$ means the stress at which the piece would fail in N number of cycles.

σ_0 is a "theoretical" value at which the piece fails in zero cycles.

k represents the damping parameter.

N is the number of cycles

The correlation factor and deviation are satisfactory, as summarized in table 3. Some curves obtained from the model are drawn in figures 9 and 10.

The difference between the σ_0 and the real σ_{max} can be attributed to the multiple tiny plasticization processes occurring in front of the crack tip while opening and closing during each cycle.

The model, and correlation factors as well as the standard deviation are written in table 3.

Ageing	σ_0	K	ρ^2	Std dev
T6	1034.0	0.1300	0.9436	0.003400
T4 immediate	839.3	0.1090	0.9335	0.000572
T4 30 days	1084.7	0.1318	0.9838	0.001243
T4 180 days	1275.3	0.1500	0.9705	0.001527
T4 540 days	1308.2	0.1519	0.9974	0.001766

Table 3 Model factors.

This model describes the alloy fatigue behaviour for the selection of ageing times used. However, a new correlation is found to approximate σ_0 as a function of the ageing time and the corresponding yield stress.

The new σ_0 model does not require a time evaluation.

The new model could be expressed as follows:

$$\sigma_{(N)} = \sigma_y * (4.389 + 0.0759 * \ln(t)) * e^{-k * \ln(N)} \quad (2)$$

Where:

$\sigma_{(N)}$ means the stress at which the piece would fail in N number of cycles.

σ_y is the yield stress at that time (t) of ageing.

t is the time of ageing.

k represents the damping parameter (from table 3).

This model fits the data with a significant accuracy, being the worst ρ^2 equal to 0.9818.

This model can be used as a basis for design, but it does not substitute the real fatigue behaviour of the alloy.

5. Aluminium welding

Welding is the process where two pieces of metal are melted with the aid of electrical, Fuel or frictional power; in other words it means the joint of two pieces of metal through a real metal crystalline blend. To create a crystalline bond, for instance, in a frictional stir welding, it is required to reach the adequate temperature to allow atom migration.

In whatever welding process, a heat input is required; so, in the surrounding welded area there is a Heat Affected Zone (HAZ), even for non-heat-treatable alloys. In the HAZ, microstructure is affected by grain coarsening, second phase dissolving, grain boundary re-precipitating, retrogressioning, and texture killing.

The best welding process should melt the faces to be joined without heating. Although it is not possible, it is necessary a better understanding of both the alloy and HAZ.

Additionally, Al-Zn-Mg alloy weldings have another nuisance called the white zone. The white zone, which occurs only in Al-Zn-Mg alloys, is a narrow area adjacent to the welding pool in the parent metal, with a likely precipitation free zone.

In age hardenable alloys, there are some special considerations to enhance their post welded resistances: Some of the factors are the joint design, parent-metal metallurgical state, toe or bulge configuration, gas shield, power source, and filler metal.

The weldability of Al-Zn-Mg alloys has some interesting details. Alloys with Cu+Zn+Mg content higher than 9% are poorly welded, between 6 and 8% are fairly welded but sensitive to stress corrosion cracking, and lower than 6% are good welded. (Mondolfo 1976)

For the same welding conditions, pulsed gas metal arc welding represents a better choice than the direct current counterpart due to its higher penetration.

Pulsed arc permit a better control on metal deposition, heat transfer, and arc stability, allowing welding on thinner plates.

The pulse frequency and duration affect considerably the post welded microstructure (Potluri et al., 1996).

Gas metal arc welding (GMAW) allows welding many plate thicknesses; however, to avoid the lack of fusion in large thicknesses, it is recommended piece preheating from 50 to 100°C

The welding procedure, parameters, and conditions are the commonly used in industrial applications.

The welding procedure used by the authors is Pulsed arc GMAW with the following parameters: Argon/Helium 75/25, filler metal AA5356, 20.5 ~ 21.5 Volts, 135 ~ 144 Amp., and travel speeds 520~530 mm/min first pass and 380 ~ 390 mm/min second pass.

5.1 Findings and analysis of the welded joint

To study the dilution of the base metal into the welding pool, a quantitative analyses using Energy-Dispersive X-rays (EDX) in a Scanning electron microscope is carried out. An EDX microanalysis of the W-B.M is plotted in figure 12.

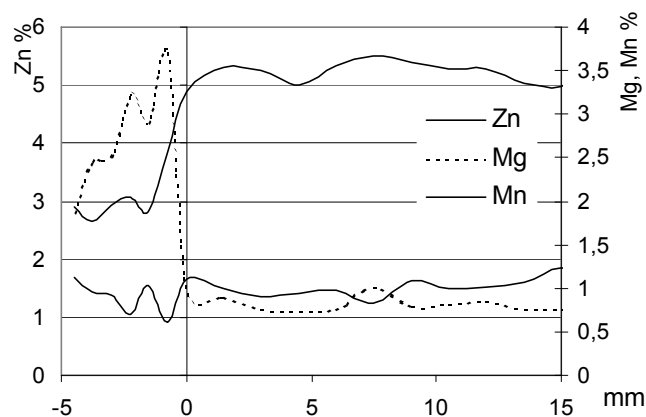


Fig. 12. EDX analysis of welded joint.

Figure 12 reveals that there is not volatilization of the alloys during the welding process, corroborating (Gomez de Salazar et al., 1998) work. Likewise, it can be seen from the same figure that there is a significant dilution of the base metal into the weld, reaching a zinc content of nearly half the one in the parent metal.

This zinc content generates a new alloy of the Al-Zn-Mg, which is corroborated by the appearance of the T precipitates $(Al,Zn)_{49}Mg_{32}$ found in the samples.

A microhardness profile of a welding joint through the HAZ is shown on figure 13

There is no evidence that the microhardness loss in the HAZ is due to a variation in the alloy contents as seen on figure 12. The microhardness defeat is attributed to a precipitation phenomenon.

The zones of possible failure, agree with the failure zones in axial and fatigue tested samples. In the microhardness profile of figure 13, five valleys appear displaying a decrease in hardness and revealing a HAZ of 24~26 mm from the fusion line. These five areas correspond to:

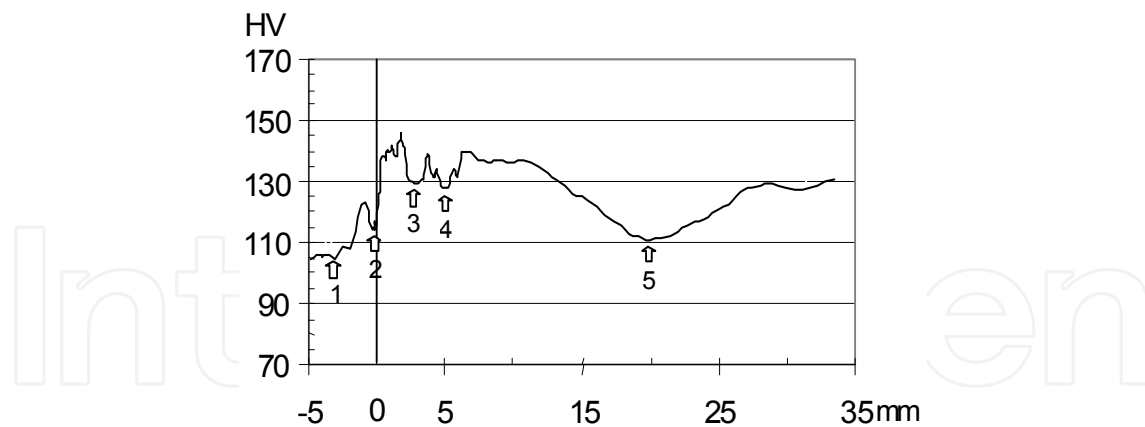


Fig. 13. Microhardness profile of welded joint and its possible failure zones.

1. The centre of the weld pool. This zone shows a decrease in hardness in the second pass welded pool of up to 40%. A much lower hardness decrease is advisable in the first pass welded pool. The hardness decrease is due to the lower alloying content of the filler metal. In the first pass, the lower hardness loss can be attributed to the thermal effects of the second pass heat input, which promotes the dissolution, diffusion and precipitation of second hardener phases, as reported by (Malin V. 1995). During the welding process, there is a dilution of the B.M into the weld. The dissolution generates a new Al-Zn-Mg-Mn alloy, as confirmed by the different analyses.
2. An adjacent zone to the interface weld pool base metal. The zone is around 0.2~1.0 mm from the interface and shows a hardness decrease of up to 34 %. This hardness decrease is the response of the internal stresses between the interface of the finer equiaxed and the large dendritic crystals. Moreover, the different cooling rates can also generate some internal stresses.
3. A zone close to the interface welded pool-base metal and in the parent metal side (HAZ). This area appears at 0.5~3 mm from the interface with a hardness reduction of up to 22 %. This area, attributed to the white zones, seems to grow further away as higher the heat input is.
4. A HAZ detected area, usually confused macroscopically with the previous discussed one. The identified zone is about 1.5 ~ 5 mm from the fusion border, but after the previous discussed one and, like the previous one, shows the same loss of hardness and also grows further away as higher the heat input is.
5. A detected zone of loss in hardness of up to 25% in the HAZ. The closest and the furthest areas can be 15 and 25 mm from the fusion line, respectively. This area is located where many authors consider a non HAZ.

It is common to find that there are three possible zones of fracture; the centre of the weld, the interface welded pool-base metal and the end surrounding of the HAZ, as reported by (Malin 1995). The non accurate zone identification can be understood due to the narrow zone where areas 2, 3 and 4 are in the weld.

To understand the mechanical behaviour, a calorimetric study of welded HAZ is performed up to 28 mm from the fusion zone, as seen on figure 14. Furthermore, a DSC running of the base metal is included to clarify the discussion.

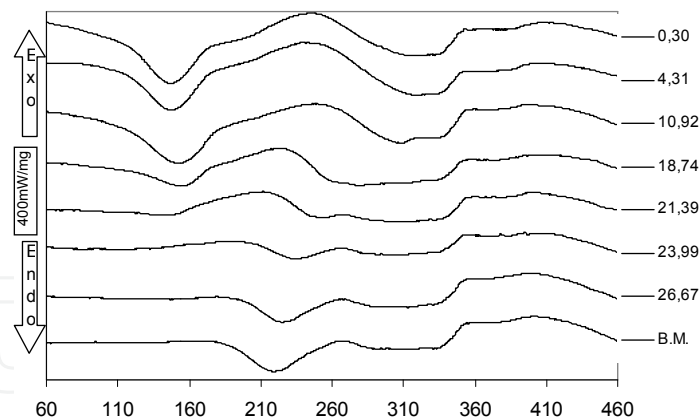


Fig. 14. DSC through a welded joint HAZ.

The calorimetric analyses reveal important details on how the precipitates evolve through the HAZ.

The analysis of the curves in figure 14 shows the presence of three peaks; one exothermic (formation) and two dissolution (endothermic) peaks. The lowest temperature (endothermic) valley corresponds to the dissolution of GPs. The first exothermic peak represents the precipitation of η' , and the second valley corresponds to the dissolution of η . The GPs dissolution energy and temperature evolution are graphed in figure 15.

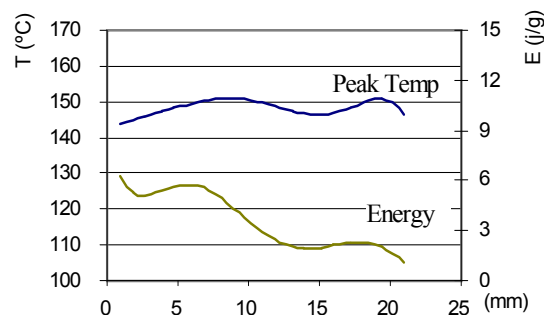


Fig. 15. Evolution of the dissolution energy and on set temperature of GPs

The evolution of the peak temperatures shows a smooth pattern, as seen in figure 14 and 15. These temperatures correspond to those referenced by researchers as (Donoso 1985, Ryum 1975).

DSC is a powerful technique for the assessment of the microstructural changes and evolution, as observed in figure 14. The evolution of the dissolution energy of the GPs shows how a total or partial dissolution of the precipitates occurs up to 12 mm. The BM has a low GP dissolution energy and does not show a formation peak, meaning that all of the alloying elements are precipitated. However, after welding, important peaks of GPs dissolution appear up to 12~15 mm.

It is important to highlight that beyond 29 mm a non HAZ is reached, as seen on figure 14. The calorimetric curves become similar to the BM curve in zones near the 30 mm from the fusion zone meaning that a non HAZ was reached.

The discussion about the dissolution and precipitation is held on the temperatures below 350°C, where the hardening precipitates GPs, η' , and η evolves.

Observing the curves near the Weld-base metal interface, a GPs dissolution occurs. Considering that this zone is so close to the heat input, there is enough energy to dissolve all the precipitates during welding, and generate some precipitates during cooling.

(Ryum 1975) proposes that the precipitates at the beginning of the HAZ are just GPs and T. However, the thermogram reveals an important amount of η and η' , and the micrograph shows the presence of at least two precipitate morphologies, corroborating the calorimetric findings.

The zone at 3 mm reveals a slightly disposition to round the spheroids, and rod-like precipitates seem to be thicker than previous ones.

This can be explained as a function of the temperature and time reached during welding.

If temperature is high enough to dissolve all the precipitates, but not long enough to allow diffusion process of the alloying elements, the precipitation on those rich alloying zones should be promote.

This corroborates Ryum's (1975) findings and is in accordance with the slight decrease on GPs energy shown in the thermograms. These rich alloying zones precipitate faster because the initial stages of the precipitation process are controlled by an interface reaction of Mg and Zn. Before welding, the initial plate state plays an important role in the final properties, due to the state of the precipitates after and before welding. Depending on the thermal state, the most thermodynamically stable plates will turn into dissolved, but with solute rich zones. On the other hand, less stable ones will dissolve precipitates and spread the solute easily. The different behaviour between both states changes completely the strength evolution.

At the 17~19 mm zone, the thermoscan reveals that from 250 to 360°C appears a joined double peak of η' and η dissolutions, denoting the existence of both precipitates.

Microhardness begins to increase at this zone, which can be attributed to the existence of both precipitates with particle sizes of ~6 nm when the Orowan mechanism begins to operate (Donoso E. 1985). On the other hand, at the 24 mm zone, the finest precipitates appear smaller than they were in the zone discussed previously. This remarkable aspect can be attributed to a real agglomeration of the alloying elements into the η' metastable phase, corresponding to the increase of the dissolution energy observed in the diagram.

The η' dissolution temperature would be lower as far the zone is from the fusion line, meaning that more unstable is that precipitate, and lower are the amount of GPs. Therefore, it can be concluded that all the alloying elements are in η' form with a tendency to transform into η (Donoso E. 1985).

At the 29 mm zone, a non HAZ is detected by DSC or microhardness response, meaning that a non affected zone is finally reached. It implies that the HAZ goes further than commonly is thought.

5.2 Mechanical behaviour of aluminium welded

As discussed above, the strength performance of aluminium welds decrease substantially, Nevertheless, there are some factors that diminish such strength loss. Leaving the toe as a reinforced zone, an increase of static strength occurs. Authors such as (Zivkovic & Anzulovic 2005) have investigated the importance of the welded surface finish. Unfortunately, many of these studies are done under laboratory conditions; i.e. untreated or mirror-like surfaces.

This section exposes the findings of welding behaviour with the commonly used industrial surface treatments after welding. A typical industrial surface treatment is seen in figure 16

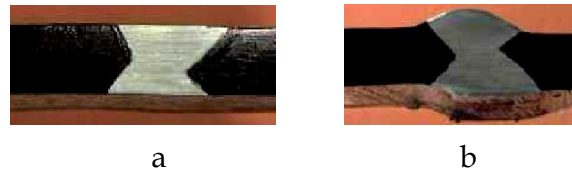


Fig. 16. Toe finish, a) toe emery eliminated, b) bulge emery smoothing.

The static mechanical properties are shown in table 4. From the table it is noted that mechanical properties of smoothed toe welds are nearly 25 % better than those of eliminated bulge welds; it is logic due to the larger cross sectional area.

The toe eliminated welds strength is lower than the bulge smoothed one. This strength difference is attributed to the microporosity of the weld pool, the worst mechanical properties of the filler metal, and the thinner cross-sectional area.

Tested samples are analyzed and microporosities are measured in the interface of parent metal-weld pools.

Microporosities are nearly spherical. It is probably because of the hydrogen separation while welding pools solidify. With a mean size of 30 ~ 50 μm , this porosity is not detected by XR non destructive tests. Although porosity affects fatigue performance, surface finishing becomes a vital parameter; notwithstanding, finishing is not a relevant factor in static strength.

Bulge condition	σ_y MPa	σ_{Max} MPa
Eliminated toe	248.3	273.6
Smoothed bulge	268.6	349.8

Table 4. Static mechanical response of welded AA7020 as toe finish.

Testing under industrial conditions is becoming more relevant each day.

In order to reproduce the real industrial conditions, the samples are welded and then just grinding with an emery to remove the toe or to smooth the toe.

The fatigue behaviour of both eliminated and smoothed bulge is observed in figure 17,

The welded fatigue strength is lower than the parent metal one; although, both strengths have the same pattern and behaviour.

Figure 17 shows that the total and partial bulge removal do not affect significantly the fatigue behaviour. However, when compared to bulge removal, toe elimination gives a higher dispersion and slightly better behaviour (~3%) in the high cycle zone ($>2 \cdot 10^6$ cycles).

It is in clear disagreeing with most of the bibliographic findings. Obviously, these dissimilarities are due to the differences in the surface roughness.

The toe dihedral angle gives an important stress concentration, which is reduced or eliminated when the toe weld is emery smoothed.

The second phases play an important role on the mechanical properties. During welding, such precipitates trial dissolution, precipitation, retrogression ageing, and overageing processes. It is advisable that the thermal state before welding plays also an important role.

Some studies are done to evaluate thermal state influence on the parent metal before welding. The thermal states selected are T6 and T4 with a 30-day natural ageing.

To evaluate the evolution of the HAZ, microhardness profiles are done and represented in figure 18.

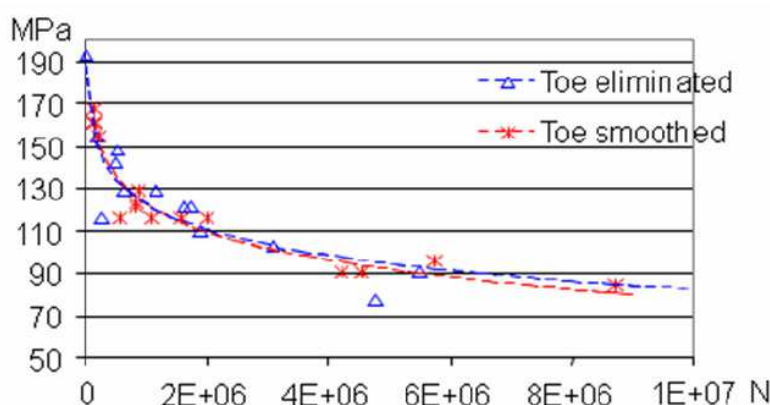


Fig. 17. Fatigue behaviour of AA7020 welding as a function of toe configuration.

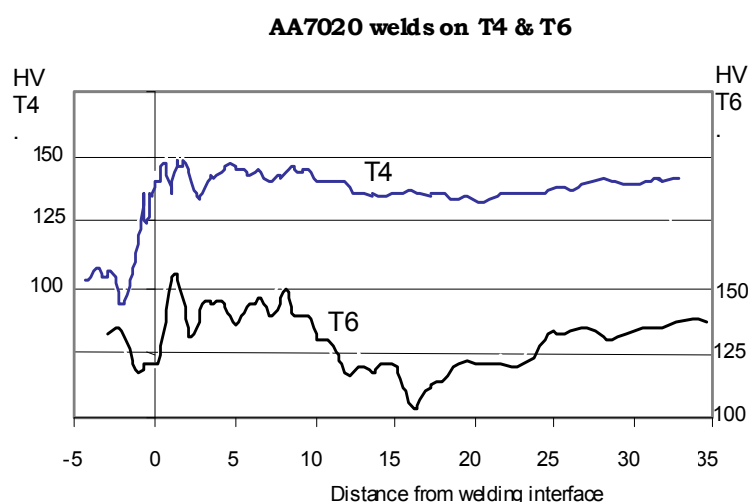


Fig. 18. Microhardness profiles on welded plates on previous T4 and T6 thermal state.

As seen in figure 18, there are some differences on the hardness behaviour. (Malin 1995, Den Ouden et al., 1999) quoted that welds of T6 plates show typical HAZ with three clearly defined areas; total dissolution and ageing, partial dissolution precipitation and overageing; for this reason, the T6 microhardness profile in figure 18 shows such kind of pattern, on the other hand, the T4 profile shows a more steady configuration because there is only dissolution and ageing through the HAZ.

The static strengths are shown in table 5

Thermal state	σ_0	σ_{Max}
T6	244,0	265,3
T4	253,3	308,9

Table 5. Static strengths of AA7020 aluminium welded in T4 and T6

As presented in table 5, there is a significant diminution of strength after welding. However, it is less notorious in welds of T4 plates, corroborating microhardness findings.

The microscopic precipitation evolution through the HAZ of both welding states is shown in figures 18 to 21.

As seen in figure 18 a) and b), there are some noticeable differences. Coarse precipitates in welds of T6 plates seem to be bigger than those in the welds of T4 plates. Additionally, the T4 welds show profuse tiny precipitates over the whole matrix. This finding corroborates the microhardness profile, where the loss of microhardness through the HAZ is lower in T4 welds.

The micrographs in figure 19 show the differences between the welds of both T6 and T4 states. Through the matrix of T6 welds, there is a heterogeneity on precipitate sizes and a lack of tiny precipitates; while in the matrix of T4 welds, there is a more uniform size of the coarse precipitates and a extended small precipitates.

In the welds of T6 plates, microhardness in the 10~13 mm zone starts to decrease considerably. On other hand, in the welds of T4 plates, microhardness does not decrease considerably; it can be intuitively understood due to the influence of the precipitations seen in figure 19 b).

In the welded zone of T6 plates, dissolution, retrogression, and ageing processes are present (Den Ouden et al., 1999). In the T4 case, just a dissolution and precipitation processes occur because of an incipient precipitation state.

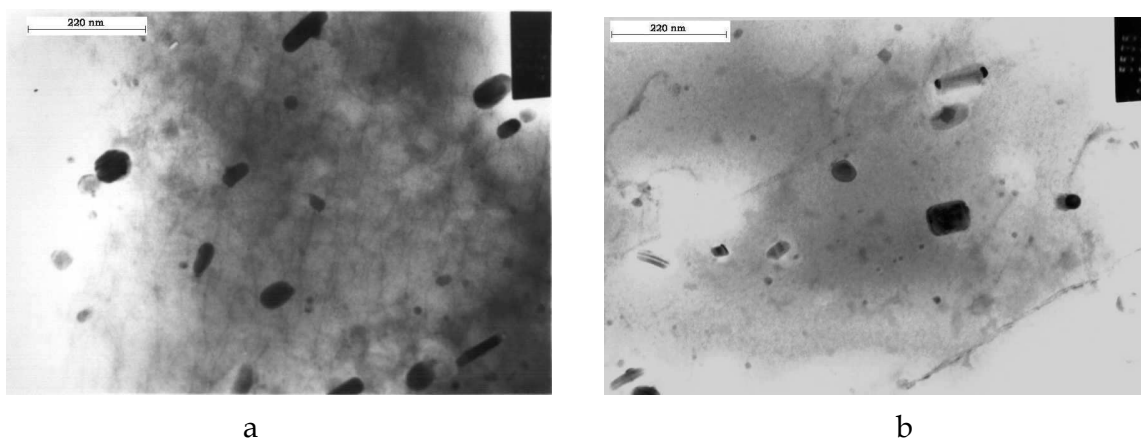


Fig. 18. TEM micrograph of AA7020 welded 46400X a) T6 at 1.9 mm from the fusion zone b) T4 at 1.5 mm from the fusion zone.

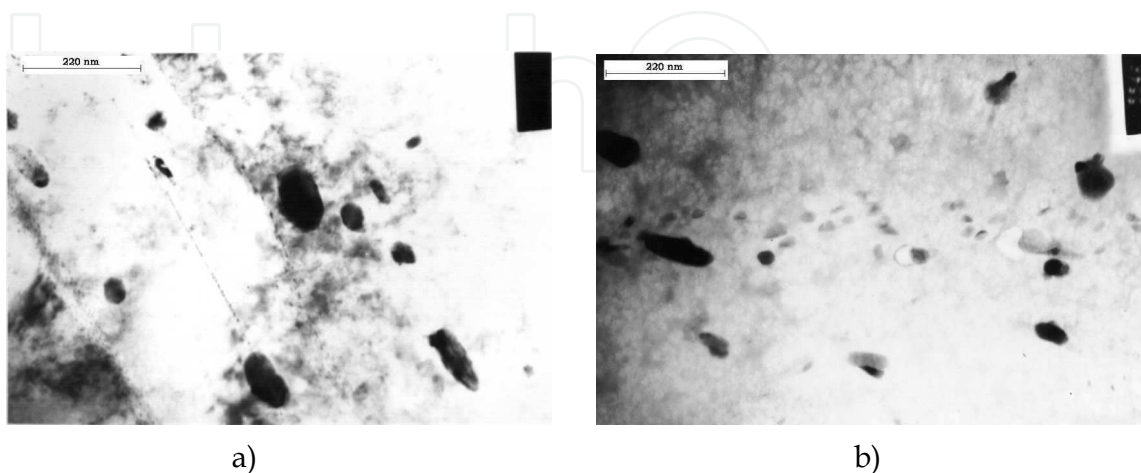


Fig. 19. TEM micrograph of AA7020 welded 46400X a) T6 at 10.8 mm from the fusion zone b) T4 at 12.5 mm from the fusion zone.

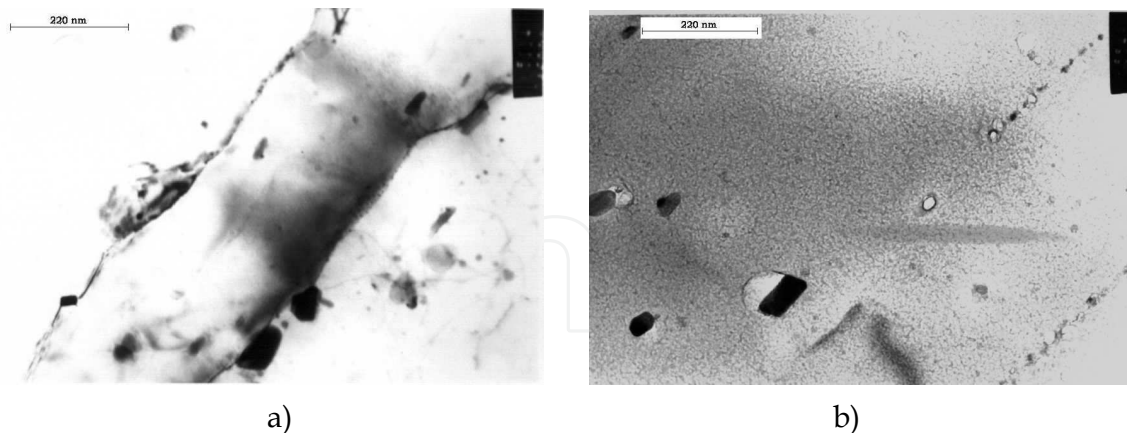


Fig. 20. TEM micrograph of AA7020 welded 46400X a) T6 at 15.1 mm from the fusion zone
b) T4 at 14.7 mm from the fusion zone.

Figure 20 shows, for the 15 mm zone of the T6 welds, large heterogeneities on precipitates are present. On the other hand, in the T4 welds, it is observed profuse tiny precipitates over the whole matrix. Another aspect to highlight is the appearance of subgrain structures and aligned bead precipitations along the subgrain borders, as seen in figures 20 a) and b).

Figures 20 b) and 21 b) demonstrate how vacancies (dislocations, in our case) play an important role in the precipitation processes and dislocations create subgrain crystalline defects. In the subgrain borders, precipitations are enhanced.

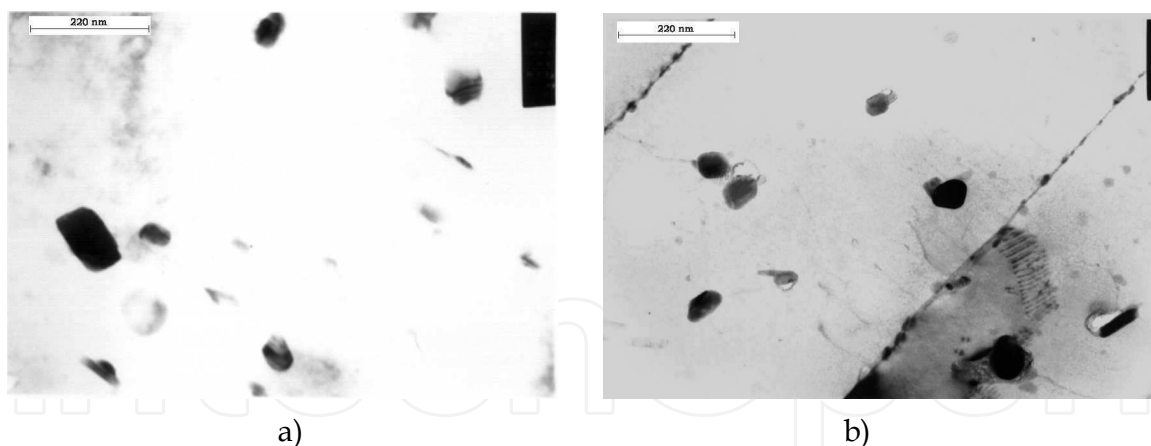


Fig. 21. TEM micrograph of AA7020 welded 46400X a) T6 at 17.9 mm from the fusion zone
b) T4 at 16.9 mm from the fusion zone.

Figure 21 a) and b) show the differences between both T6 and T4 microstructures, respectively

In the T6 weld shows coarser precipitates and a lack of tiny ones. In the case of T4 welds, it is shown evidences of fine precipitates through the matrix.

The fatigue behaviour in figure 22 shows a better performance on T4 welds; as expected because of its precipitate homogeneity.

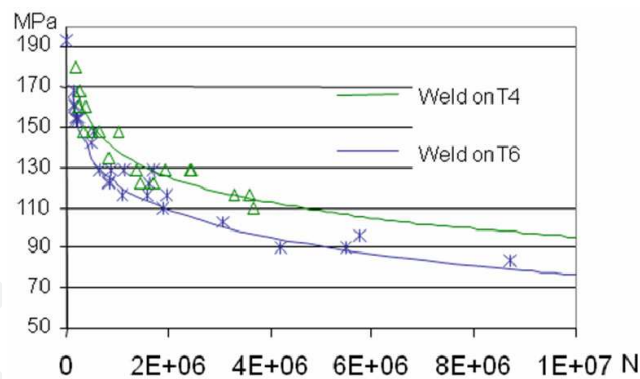


Fig. 22. Fatigue behaviour of AA7020 welding as a function of parent metal's thermal state.

5.3 AA7020 welded fatigue behaviour mathematical model

The following mathematical model for the fatigue behaviour of T4 and T6 welded plates is proposed.

$$\sigma_{(N)} = \sigma_y * (K_1 + (3.005 * K_2 * K_3)) * e^{-(k_3/a) * \ln(N)} \quad (3)$$

Where:

$\sigma_{(N)}$ is the fatigue strength for the number of cycles (N)

σ_y is the yield point.

K1 is the constant of thermal state of the parent metal.

K2 is the damping coefficient associated to the thermal state of parent metal.

K3 is the toe improvement factor.

a is the factor that involves the welding procedure in this case is 14.309

K1	Parent metal T6	- 3.0
	Parent metal T4	- 2.05
K2	Parent metal T6	1.0
	Parent metal T4	0.85
K3	Toe eliminated	1.636
	Toe smoothed	1.48

Table 6. Factor of the AA7020 welded fatigue model.

The general AA7020 welded fatigue model (3) with the factors in table 6 fits quite good the experimental data.

6. Conclusion

The further studies over the engineering materials, the better understanding of it. It allows us to understand its nature and exploit its potential usability.

There are enough evidences, as presented in figure 3, that there is a precipitate precursor before the GPs, with stability under the 95°C.

Due to the precipitation evolution evaluated up to 6 years of natural ageing, there is adequate data to conclude that the only responsible of strength increase due to ageing is the GPs instead of the normally thought η' .

Although the definition of T6 is solution heat treatment and then artificial aged, commercial plates on T6 still preserve part of their lamination texture. Therefore, special care must be taken when such plates are used in applications involving strength and fatigue.

The best balance between time and strength in artificial ageing for AA7020 alloys is the temperature of 122°C for 48 hours.

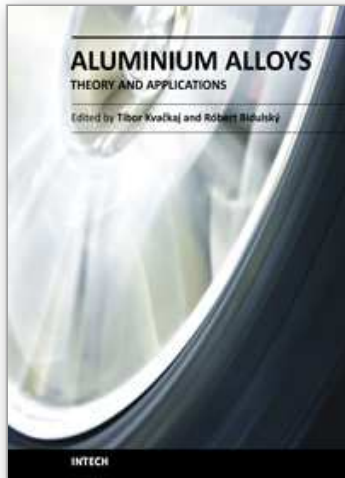
AA7020 alloys are low in copper and do not exhibit real sensitive to quench severity in the T6 heat treatments. Nevertheless, water quenching delays overageing.

Three different models were proposed for mechanical response under fatigue loading conditions. These models fit quite well the experimental data and should be used just for preliminary designs.

The authors wish to thanks the microscopy service of the Universidad Politecnica de Valencia and Dr Jose A. Alvarado for his help reviewing this manuscript.

7. References

- Alubook. (July 2010) <http://www.alu-info.dk/html/alulib/modul/albook40.htm>,
- Den Ouden T. Ma (1999) Softening behaviour of Al-Zn-Mg alloys due to welding *Material science and engineering A266*, 1999, pp198-204
- Donoso, E. (1985) Calorimetric study of the dissolution of Guinier-Preston Zones and n' Phase in Al-4.5at%Zn-1.75at%Mg. *Material Science and engineering*, vol 74, pp 39-46
- Gatto, F., Morri, D.(1979) Fatigue behaviour of some welded joints of aluminium alloys. Ed Novara. Italy.
- Gomez de Salazar, J.M, A. Ureña, E. Villauriz, S. Manzanedo E I. Barrena. (1998) Soldadura TIG y MIG de las aleaciones de aluminio 6061 y 7020. Estudios microestructurales y de propiedades mecanicas. *Revista Metalurgia*. vol, 34 pp 276, 280
- Jiang-hai, Y.; Sheng-dan, L.; Xin-ming, Z. and Xiao-yan, Z. (2008) Effect of Two-Step Ageing on Microstructure and Properties of 7150 Aluminium Alloy *Chinese Journal of Rare Metals* Volume 15, Number 2, 153-158
- Malin V. (1995) Study of the metallurgical phenomena in the HAZ of 6061-T6 Aluminium welded joints *Welding research supplement* pp 305-318
- Mondolfo, L.F.(1976) *Aluminium Alloys: Structure and Properties*. Ed. Butterworths, London-Boston.
- Polmear, I. J. (1996) Recent developments in light alloys Overview *Materials Transactions JIM*, Vol 37, N° 1, pp12, 31
- Potluri N. Gosh P.Gupta P., and Srikanth R. Y. (1996) Studies on weld metal *Welding journal* Vol 74 1996 pp 64
- Robinson, J. S.; Tanner, D. A. (2006) The Influence of Aluminium Alloy Quench Sensitivity on the Magnitude of Heat Treatment Induced Residual Stress *Journal Materials Science Forum* (Volumes 524 - 525) Residual Stresses VII pp. 305-310
- Ryum, N. (1975) Precipitation kinetics in an Al-Zn-Mg alloy". *Zeitschrift fur Metalkunde*. Vol 64. Pp 338 343
- Schiller, I.; Gubicza, J.; Kovács, Zs.; Chinh, N. Q.; and Illy, J. (2006) Precipitation and mechanical roperties of supersaturated Al-Zn-Mg alloys processed by severe plastic deformation *Materials Science Forum* Vols. 519-21 pp. 835-840
- Soto, J. L.; Campillo, B.; Juarez-Islas, J.A. (2007) Prediction of Microstructure and distribution of Solute in Al-Zn-Mg Non-Dilute Alloys *Materials Science Forum* (Volume 560) Advanced Structural Materials III PP 73-78
- Zivkovic, D. & Anzulovic, B. (2005) The fatigue of 5083 aluminium alloy welds with the shot-peened crater hot-cracks *Materials and. Design*. 26 n°3 pp 247-250.



Aluminium Alloys, Theory and Applications

Edited by Prof. Tibor Kvackaj

ISBN 978-953-307-244-9

Hard cover, 400 pages

Publisher InTech

Published online 04, February, 2011

Published in print edition February, 2011

The present book enhances in detail the scope and objective of various developmental activities of the aluminium alloys. A lot of research on aluminium alloys has been performed. Currently, the research efforts are connected to the relatively new methods and processes. We hope that people new to the aluminium alloys investigation will find this book to be of assistance for the industry and university fields enabling them to keep up-to-date with the latest developments in aluminium alloys research.

How to reference

In order to correctly reference this scholarly work, feel free to copy and paste the following:

Carlos Bloem, Maria Salvador, Vicente Amigó and Mary Vergara (2011). Aluminium 7020 Alloy and Its Welding Fatigue Behaviour, Aluminium Alloys, Theory and Applications, Prof. Tibor Kvackaj (Ed.), ISBN: 978-953-307-244-9, InTech, Available from: <http://www.intechopen.com/books/aluminium-alloys-theory-and-applications/aluminium-7020-alloy-and-its-welding-fatigue-behaviour>

INTECH
open science | open minds

InTech Europe

University Campus STeP Ri
Slavka Krautzeka 83/A
51000 Rijeka, Croatia
Phone: +385 (51) 770 447
Fax: +385 (51) 686 166
www.intechopen.com

InTech China

Unit 405, Office Block, Hotel Equatorial Shanghai
No.65, Yan An Road (West), Shanghai, 200040, China
中国上海市延安西路65号上海国际贵都大饭店办公楼405单元
Phone: +86-21-62489820
Fax: +86-21-62489821

© 2011 The Author(s). Licensee IntechOpen. This chapter is distributed under the terms of the [Creative Commons Attribution-NonCommercial-ShareAlike-3.0 License](#), which permits use, distribution and reproduction for non-commercial purposes, provided the original is properly cited and derivative works building on this content are distributed under the same license.

IntechOpen

IntechOpen